Microtomography of Systems at High Pressure II: Characterization of an Opposed-anvil High-pressure Cell for *In Situ* Microtomography

T. Uchida, Y. Wang, M.L. Rivers, S.R. Sutton, F. Westferro, J. Gebhardt
Consortium for Advanced Radiation Sources, The University of Chicago, Chicago, IL, U.S.A.

Introduction

We have been developing techniques for synchrotron microtomographic imaging under high pressure and temperature. The most critical issue in performing tomography experiments under high pressure is the limited x-ray access to the sample because of the highly absorbing materials, such as tungsten carbide and tool steel, that are typically used in generating pressure. To avoid this problem, we employ an opposed-anvil high-pressure cell, sometimes referred to as the Drickamer cell, that possesses some unique features when compared to a diamond anvil cell (DAC) and conventional multianvil apparatus. The sample is compressed between two opposed anvils, similar to what occurs in a DAC. However, the relatively large volume of the sample chamber in the Drickamer cell permits the use of resistive heating for melting experiments, which allows us to observe dynamic processes at a high pressure and high temperature, which may further our understanding of the formation of the Earth's core. X-ray transparent containment rings give easy access to the sample.

In this report, we focus on the development and characterization of the Drickamer cell and examine its x-ray diffraction and imaging capabilities for application to high-pressure microtomography. We also discuss the possibility of using the Drickamer cell for measuring other physical property of melts, such as radial distribution function and density.

Methods and Materials

Figure 1 shows a schematic of the Drickamer cell, consisting of top and bottom tungsten carbide (WC) anvils and a containment ring, which is made of x-ray-transparent materials, such as aluminum alloy or silicon carbide. The gap between the two anvils is filled with a pressure medium, made of a mixture of boron and epoxy resin (BE), that is also transparent to x-rays.

To examine pressure generation and x-ray diffraction capabilities, the Drickamer cell was loaded into a 250-ton press installed at the sector 13 bending magnet beamline at the APS. Powdered NaCl was loaded in the sample chamber in the middle of the BE cell. By using the equation of state of NaCl [1], the pressure was calculated from the lattice strains of NaCl during the compression and

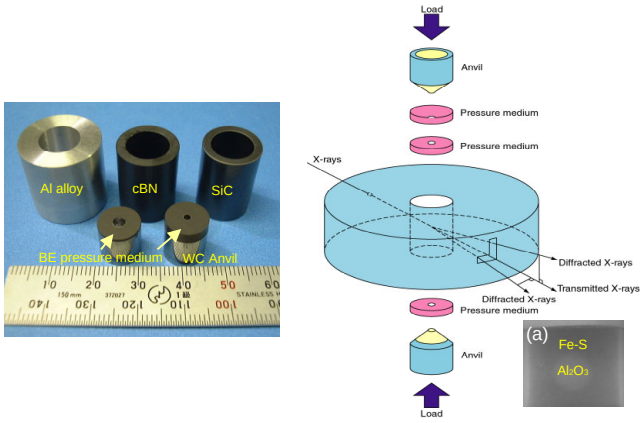

FIG. 1. Drickamer cell. Two opposed anvils compress the sample. The containment ring can be made of aluminum alloy, cubic boron nitride (cBN), or silicon carbide (SiC). The low absorption of the pressure medium and containment ring allows a wide 2θ range for x-ray access. When sintered diamond is used as the anvil material, the pressure range can be extended to more than 50 GPa. Photographic inset is an example of image.

decompression cycle. White x-radiation was used with a Ge single-element solid-state detector to measure lattice strains of NaCl at a fixed 2θ angle of 5.5° based on the energy-dispersive method. We tried several different anvil geometries by varying the following parameters: (1) outer diameter of anvils (10 and 20 mm); (2) diameter of top surface (2.5, 3.0, and 3.5 mm); and (3) tapering angle from top surface (10° and 20°).

To examine the imaging capability, tomographic data [2] were collected for the entire cell assembly (including the outer containment ring and the pressure medium). The sample was a 0.5-mm alumina sphere embedded in a mixture of Fe and FeS_2 powders (containing 9-wt% S). Data collection was conducted at the same experimental station (13-BM-D). The energy of the monochromatic x-ray beam was 40 keV, based on optimizing the image contrast between the alumina sphere and surrounding Fe-S alloy. The transmitted x-rays were imaged with a single-crystal yttrium-aluminum-garnet (YAG) scintillator (0.2-mm thick), a microscope objective, and a 1242×1152-pixel fast charge-coupled device (CCD) detector. The field of view

was approximately 9×8 mm, which resulted in a spatial resolution of about 13.3 μm, after 2×2 binning. Over 720 x-ray projections were collected by rotating the sample through 180°. Then tomographic reconstructions were performed by using filtered backprojection for all of the angles in a given row.

Results and Discussion

Figure 2 shows a representative x-ray diffraction pattern. Good statistics were obtained for NaCl for a 200-second counting time. Lattice contamination from the heating material (graphite) is seen.

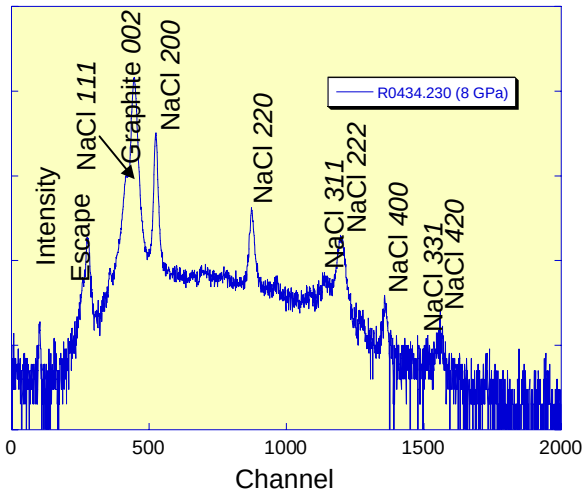

FIG. 2. Representative x-ray diffraction pattern from run R0434 (#230). Exposure time was 200 seconds. Five diffraction peaks (200, 220, 222, 400, and 420) are available for pressure measurement.

Figure 3 shows the pressure efficiency with various anvil geometries. Larger anvils (20 mm in diameter) have a low efficiency but allow more load to be applied. As a result, the maximum pressure reached is higher than that of any 10-mm anvils. However, larger anvils contain more pressure mediums in the x-ray beam path, which may raise the noise level in x-ray images. Thus, in terms of x-ray diffraction, the current setup works very adequately, making it possible to measure radial distribution functions for melts.

When anvils have the same diameter, those with a smaller tip surface or steeper tapering angle show more efficiency (Fig. 3). However, a steeper slope means a larger pressure gradient, so the pressure condition is less stable; experiments often end with a blow-out (Fig. 4). The pressure, not the load, at which the blow-out happened was reproducible (at 6.6 GPa). These blow-outs are strongly linked to the strength of the Al-alloy containment ring. Figure 4 shows that blow-outs caused brittle failure of the containment ring rather than ductile deformation.

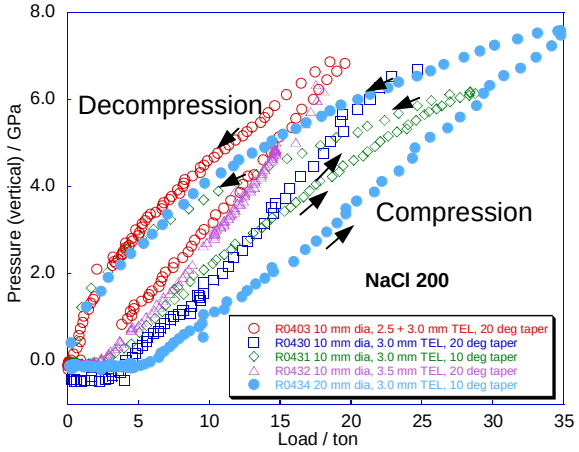

FIG. 3. Pressure efficiency of the tomographic Drickamer cell. The larger anvil lowered the efficiency but allowed more load to be applied. The smaller tip surface and steeper tapering angle increased efficiency, but experiments often ended with a blow-out.

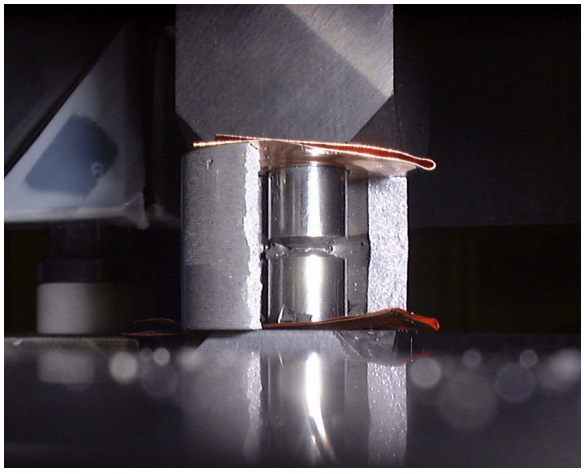

FIG. 4. Photograph taken after blow-out in run R0430 (at 24 tons). Brittle failure occurred in the Al-alloy containment ring. Anvils recovered are still usable.

Figure 5 compares reconstructed slices of alumina sphere and Fe-S alloy in the horizontal direction with various containment rings, although these rings cannot be seen in the images because of large magnification. All slices were prepared at the same height, enabling direct comparison of the effect of containment rings. With SiC [Fig. 5(c)] and cBN [Fig. 5(d)] rings, boundaries between the alumina sphere and Fe-S alloy and between the Fe-S alloy and the pressure medium became a little blurred. The fuzziest image was obtained with the Al-alloy ring [Fig. 5(b)]. To quantify the fuzziness, these images were filtered by a certain intensity range (Fig. 5, right column). The number of pixels in this intensity range was then counted,

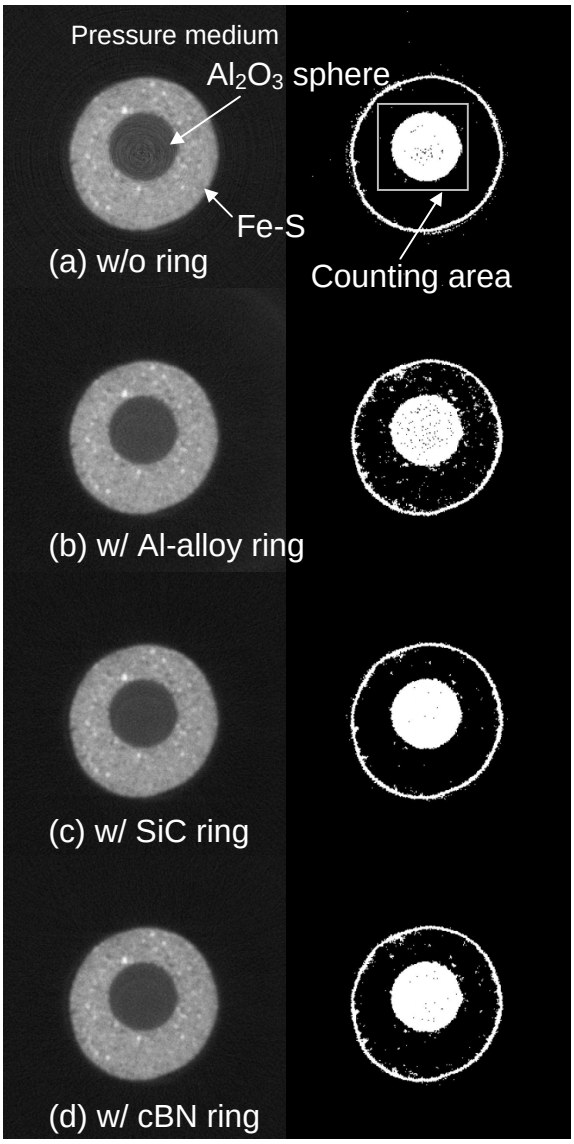

FIG. 5. Comparison of reconstructed slices (a) without any rings, (b) with a 5-mm-thick Al-alloy ring, (c) with a 2-mm-thick SiC ring, and (d) with a 2.5-mm-thick cBN ring. The left column shows reconstructed slices, while the right shows filtered images to count the number of pixels (white dots). The ring artifact is removed by limiting the counting area, which is indicated by a gray rectangle.

corresponding to a volume measurement. However, filtering the data could not remove ring artifacts caused at the boundary between the Fe-S alloy and the pressure medium (Fig. 5, right column). To remove this artifact, we constrained a counting area by a rectangular parallelepiped.

The number of pixels is summarized in Table 1. Al-alloy caused about 10% of the error in the volume measurement, which is mainly due to noise outside the sphere [Fig. 5(b)]. The 10% error can be regarded as a run-to-run-basis error.

TABLE 1. Effect of ring material (on top row) on volume measurements (number of pixels, bottom row).

No Sleeve	Al-Alloy	SiC	cBN
253,365 (standard)	280,038	265,358	269,664

Compared to Al-alloy, the errors with SiC and cBN rings are relatively small (about 5%).

The number of pixels is largely affected by the intensity range selection. Table 2 summarizes the effect of this range selection on counting the number of pixels. Figure 6, which corresponds to Table 2, compares the images processed. If the upper bound is high, the image picks up noise outside the sample [Fig. 6(b)]. As the upper bound is lowered, outside noise decreases [Fig. 6(c) and 6(d)]. We should establish a criterion to optimize the upper and lower bounds to minimize error. A better selection of bounds is critical to obtaining reliable numbers.

TABLE 2. Effect of selected intensity range for the run measured with Al-alloy containing ring (top row) on volume measurements (number of pixels, bottom row).

300-1500	300-1300	100-1100
5,550,689	4,545,852	4,147,261

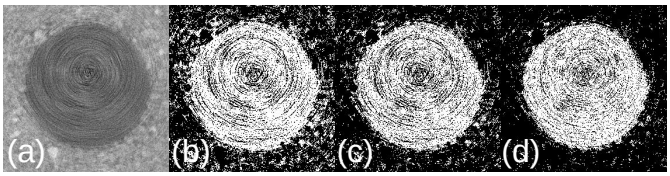

FIG. 6. Effect of filtering on reconstructed images. (a) Original reconstructed slice. (b) The image with intensities between 300 and 1500. (c) The image with intensities between 300 and 1300. (d) The image with intensities between 100 and 1100.

Discussion

The current tomographic Drickamer setup is usable for obtaining robust data for x-ray diffraction. The exposure time was 200 seconds, which is shorter than times used in typical DIA and T-cup experiments. The x-ray diffraction capability enables many kinds of experiments, including the measurement of radial distribution functions for melts.

X-ray images indicate that volume measurements of the sample are valid as long as the comparison of volumes is conducted in the same run, because error is cancelled. For example, measurement of the volume change between the

solid phase and liquid phase can be carried out by using the current setup. In order to compare densities obtained from different runs or to observe microtexture, more study is required to reduce the error that can be seen in Fig. 5. We will try to make a more uniform flatfield and develop a method that reduces noise by establishing a 3-D curve-fit or another method of this kind.

Acknowledgments

We thank N. Lazarz, F. Sopron, M. Jagger, G. Shen, V. Prakapenka, M. Newville, P. Eng, J. Pluth, and C. Pullins for their valuable contributions. Work performed at GSECARS is supported by the National Science Foundation (Earth Sciences), U.S. Department of Energy (DOE, Geosciences), W.M. Keck Foundation, and U.S. Department of Agriculture. Use of the APS was supported by the DOE Office of Science, Office of Basic Energy Sciences, under Contract No. W-31-109-ENG-38.

References

[1] D.L. Decker, J. Appl. Phys. **42**, 3239-3244 (1971).
[2] M.L. Rivers, S.R. Sutton, and P. Eng, in *Developments in X-ray Tomography II*, edited by U. Bonse (International Society for Optical Engineering, Bellingham, WA, 1999), pp. 78-86.